COMMUNICATION

Surfactant-Stripped Frozen Pheophytin Micelles for Multimodal Gut Imaging

Yumiao Zhang, Depeng Wang, Shreya Goel, Boyang Sun, Upendra Chitgupi, Jumin Geng, Haiyan Sun, Todd E. Barnhart, Weibo Cai, Jun Xia, and Jonathan F. Lovell*

Multimodal imaging is being advanced clinically and preclinically to provide improved biomedical diagnosis with combined and complementary information.[1,2] A wide range of hybrid imaging modalities have been investigated including positron emission tomography (PET) based multimodalities (e.g., PET/magnetic resonance imaging (MRI),[3] PET/fluorescence imaging (FL),[4] PET/MRI/photoacoustic computed tomography (PACT),[5,6] MRI based multimodalities (e.g., MRI/CT/upconversion,[7] MRI/FL[8]), and CT fused modalities (e.g., CT/MRI/FL,[9] CT/PET/single photon emission computed tomography,[10] CT/PET[11,12]) as well as combinations with phototherapies for image-guided treatments.[13,14] Concurrently, numerous nanoparticles have been designed as contrast agents with improved properties in various imaging modalities. Some examples include superparamagnetic iron oxide nanoparticles, gold nanoparticles,[15–17] polymeric nanoparticles,[18–22] liposomes,[23–25] and upconversion nanoparticles.[26–29] However, multimodal imaging has not been frequently explored for imaging the intestine, possibly due to the harsh chemical conditions of the gut. CT, MRI, or ultrasound based modalities for intestinal imaging are limited by drawbacks such as radiation exposure, cost, safety concerns, or lack of suitable contrast. A gut imaging contrast agent would benefit from the following: 1) being edible and generally regarded as safe; 2) transiting stably through the intestine; and 3) activity in multiple modalities.

Y. Zhang, D. Wang, U. Chitgupi, J. Geng, Prof. J. Xia,
Prof. J. F. Lovell
Department of Biomedical Engineering
University at Buffalo
The State University of New York
Buffalo, NY 14260, USA
E-mail: jflovell@buffalo.edu
Y. Zhang, B. Sun, Prof. J. F. Lovell
Department of Chemical and Biological Engineering
University at Buffalo
The State University of New York
Buffalo, NY 14260, USA
S. Goel
Materials Science Program
University of Wisconsin–Madison
Madison, WI 53705, USA
H. Sun, Prof. W. Cai
Department of Radiology
University of Wisconsin–Madison
Madison, WI 53705, USA
Dr. T. E. Barnhart, Prof. W. Cai
Department of Medical Physics
University of Wisconsin–Madison
Madison, WI 53705, USA

Recently, we developed a surfactant-stripping strategy using hydrophobic naphthalocyanine (Nc) dyes, generating surfactant-stripped induced frozen micelles (ss-InFroMs).[30–32] The process makes use of Pluronic surfactant, which is converted to unimeric form at low temperatures, and is then selectively stripped away with low temperature membrane processing, leaving behind ss-InFroMs with extremely high optical absorption in the near infrared. This approach provided contrast for functional PACT of intestine.[30] PET for whole body intestinal imaging was also possible by simple incubation with the ^{64}Cu ($t_{1/2}$ = 12.7 h) radioisotope which chelates in the center of Nc macrocycle and the Nc ss-InFroMs are thereby an intrinsic chelator.

Although gut imaging using Ncs is promising, there are potential limitations. For example, fluorescence imaging of intestine was not possible with this approach due to the self-quenching of the extremely hydrophobic dyes. Optical fluorescence imaging, which offers the advantages of low cost, high speed, and good resolution, has been shown to be possible for functional imaging of intestinal peristalsis in mice.[33] More significantly, even though Ncs were found to be nearly completely excreted in feces, safety concerns might arise for administering a dye that is not naturally occurring and has not been extensively tested in humans. Porphyrin-related molecules are naturally occurring and have numerous applications for imaging and therapy.[34,35] Here, we demonstrate that demetallated chlorophyll-*a* (Chl); pheophytin-*a* (Pheo), which is already present in human diets, can be used for noninvasive, nonionizing trimodal intestinal imaging with FL, PA, and PET. Chl is found in various green vegetables such as spinach[36] and green beans,[37] which contain about 0.125% and 0.0045% total mass of Chl, respectively. In this study, Pheo ss-InFroMs were administered in a small volume to mice at a dose corresponding to 82.2 g spinach per kg body weight or 2.3 kg green beans per kg weight, respectively.

As shown in **Figure 1**a, Chl was converted to Pheo after the dechelation of magnesium in acidic conditions. The displacement of the metal was accompanied by changes in absorbance, with a blue shift of the Soret band (from 428 to 408 nm), a red shift of the longest Q band (from 660 to 665 nm), and restoration of two other Q bands (between 500 and 550 nm) (Figure 1b).[38] Mass spectrum analysis showed the product had only one single peak, corresponding to the expected Pheo mass (Figure S1, Supporting Information). Following magnesium removal, Pheo migrated further than Chl on thin layer silica gel chromatography (data not shown), showing it has less polarity, which is in agreement with the simulated octanal:water log *P* partition values of Chl and Pheo as predicted by the ALOGPS algorithm.[39] This is noteworthy since we previously showed that more hydrophobic dyes generally give rise to more stable induced frozen Pluronic micelles.[30]

Materials
Views
www.MaterialsViews.com

ADVANCED
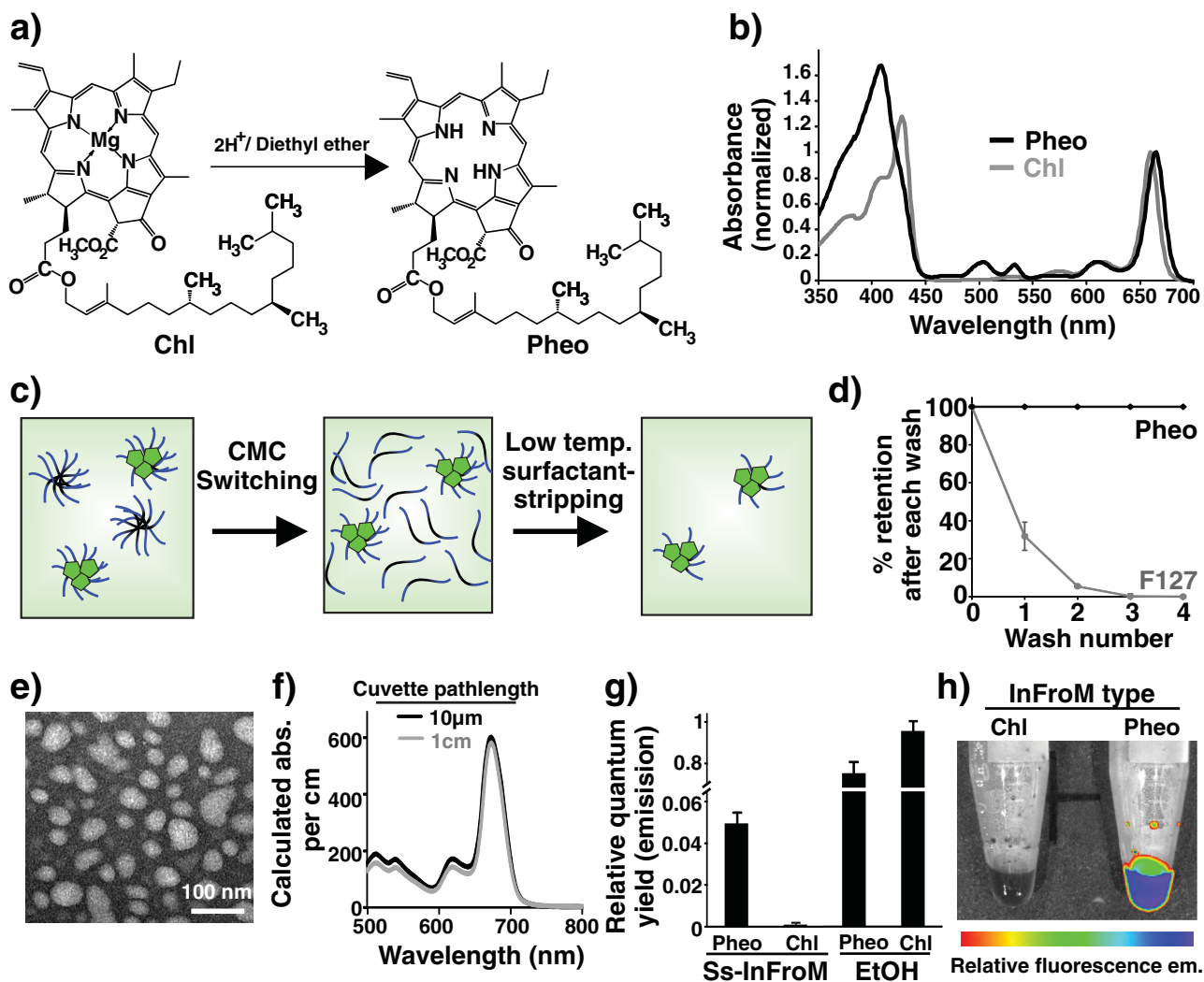MATERIALS
www.advmat.de

COMMUNICATION

Figure 1. Preparation of Pheo ss-InFroMs. a) Generation of pheophytin-*a* (Pheo) from chlorophyll-*a* (Chl). b) Q-band normalized absorbance of Chl and Pheo in chloroform. c) Schematic illustration of Pheo ss-InFroM preparation by low-temperature surfactant stripping. The dye, the F127 hydrophobic segment, and the F127 hydrophilic segment are shown in green, black, and blue, respectively. d) Pheo (black) and F127 (grey) retention with increasing centrifugal filtration washes at 4 °C. e) Negatively stained transmission electron micrograph of Pheo ss-InFroMs. f) Calculated absorbance (per cm) of aqueous Pheo ss-InFroMs measured in a cuvette with either a light path of 10 mm after a thousand fold dilution, or a 10 μm light path without dilution. g) Relative fluorescence quantum yields of Pheo and Chl in ss-InFroM form or in ethanol. h) Fluorescence image of Chl and Pheo ss-InFroMs. Error bars show mean +/− std. dev. for n=3.

Next, Pheo ss-InFroMs were made by low temperature surfactant stripping. Pheo was dissolved in dichloromethane (DCM) and was added to a 10% Pluronic F127 (F127) aqueous stirred solution. As the organic solvent evaporated, hydrophobic dyes were driven into the hydrophobic core of Pluronic micelles. At lower temperature, free or loose Pluronic in micelles without cargos loaded changed to unimeric form, which could be effectively removed by centrifugal filtration methods as illustrated in Figure 1c. No Pheo was found in filtrates (Figure 1d), indicative of 100% yield for Pheo in ss-InFroMs. Pheo ss-InFroMs were obtained with diameter of about 55 nm, as shown by negative stained transmission electron microscopy (Figure 1e), which is in agreement with dynamic light scattering measurement (53.7 nm, albeit with a polydispersity index of 0.38). The dye extinction

coefficients in acetone or ss-InFroM form were calculated to be 5.28×10^4 and 4.36×10^4 M^{-1} cm^{-1}, respectively, suggesting dense arrangement of dye and good solubility in micelles (Table S1, Supporting Information). Even though Pheo itself has a smaller extinction coefficient than that of gold nanorods (which are on the order of 10^8–10^9 M^{-1} cm^{-1}),[40] each ss-InFroM can load thousands of dyes, leading to a large value of absorption cross-section. The molar ratio of Pheo to F127 is 4.97 and based on geometrical estimations, each ss-InFroM contains about 1.5×10^4 dyes, yielding an optical cross-section of 2.5×10^{-12} m^2 (Table S1, Supporting Information). X-ray powder diffraction (XRD) analysis of freeze-dried Pheo ss-InFroMs did not show any dye crystallinity, suggesting that Pheo was packed irregularly without forming crystals (Figure S2, Supporting Information).

By using the temperature-sensitive critical micellization concentration switching and surfactant-stripping method, Pheo ss-InFroMs could be concentrated without noticeable shifting of absorption peak positions as shown in Figure 1f via absorbance measurements of a concentrated solution using a 10 μm light path length and a 1000-fold dilution of the same solution using a 1 cm light path length. Fluorescence of Pheo and Chl ss-InFroMs was examined. Chl ss-InFroms were nonfluorescent, as expected for a densely packed dye. However, Pheo ss-InFroMs were found to retain a substantial relative fluorescence quantum yield (Figure 1g and Supplementary Figure 3). Presumably, the displacement of the central metal changed the interaction between the dye and F127, altering the packing of dyes in the micelles, leading to greater micelle fluorescence of Pheo compared to Chl. This phenomenon is illustrated with fluorescence imaging of ss-InFroms as shown in Figure 1h.

Despite being much brighter than Chl, Pheo fluorescence in ss-InFroMs remained largely quenched relative to the pigment in ethanol, where it would be fully solvated without intermolecular interactions to induce quenching. Further investigations are warranted to better explain this phenomenon.

The suitability of Pheo ss-InFroMs for intestinal imaging was assessed in vitro and in vivo. First, the presumed stability of the contrast agents in the GI tract was evaluated using simulated intestinal fluid (SIF). As shown in **Figure 2**a, after incubation with SIF at 37 °C for 24 h, Pheo ss-InFroMs were stable under harsh conditions in SIF without appreciable loss of absorption. Under the same experimental conditions, Chl ss-InFroMs were not as stable as Pheo, exhibiting a significant loss of absorption, similar to gold nanorods as we previously demonstrated.[30] In vivo tests were conducted on mice orally administered 100 O.D. of the two contrast agents, respectively. Pheo was recovered
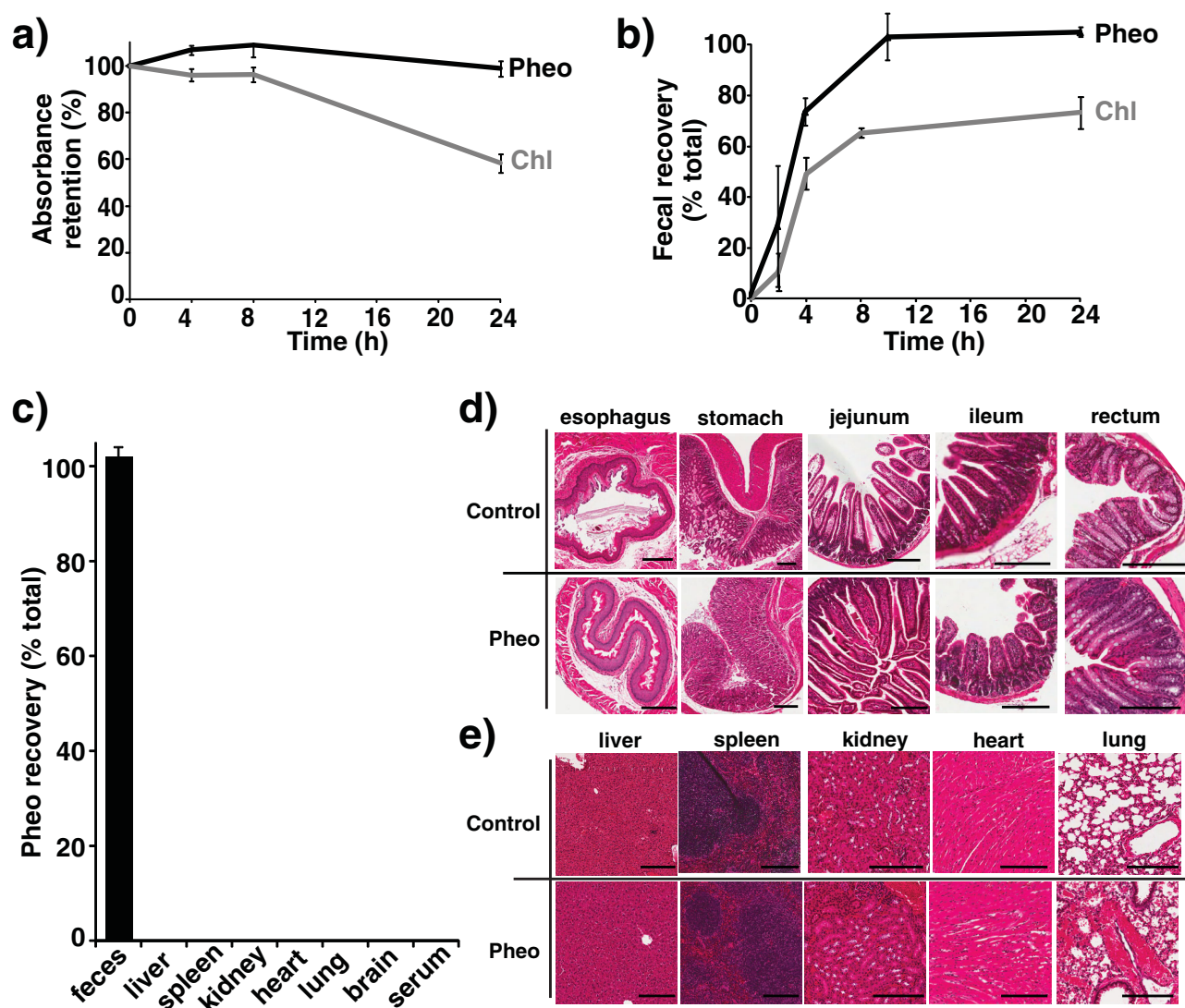

Figure 2. Intestinal stability and gastrointestinal clearance of Pheo ss-InFroMs. a) Retention of Chl and Pheo ss-InFroM absorbance during dialysis in simulated intestinal fluid. b) Cumulative recovery in feces within 24 h after gavage of 100 O.D. of Chl or Pheo ss-InFroMs. c) Biodistribution of Pheo ss-InFroMs 24 h following gavage of 100 O.D. Pheo ss-InFroMs were fully excreted in feces. Error bars show mean +/− std. dev. for n=3. No noticeable acute histopathological toxicity was induced by Pheo ss-InFroMs in d) GI or e) other organs. All scale bars represent 200 μm.
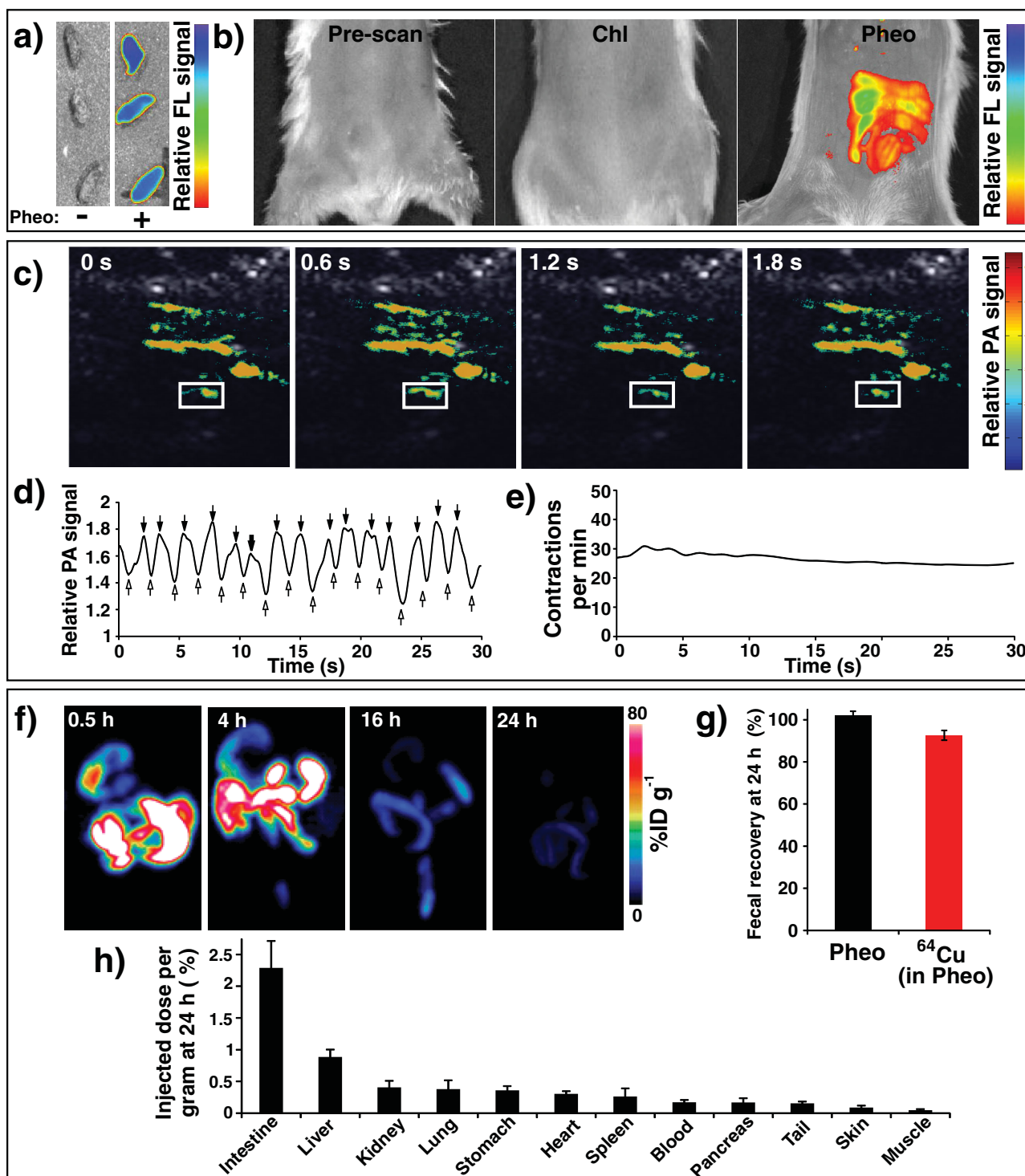
Figure 3. Trimodal gut imaging using Pheo ss-InFroMs. a) Fluorescence images of feces with and without administration of 100 O.D. Pheo ss-InFroMs. b) Fluorescence images of mice after gavage of PBS (left), 100 O.D. of Chl ss-InFroMs (middle), or 100 O.D. of Pheo ss-InFroMs (right). c) Photoacoustic images of the gut after gavage of 100 O.D. of Pheo ss-InFroMs. Photoacoustic signal is shown in color overlaid on ultrasound gray scale images. d) Fluctuation of photoacoustic signal in the region of interest (ROI, indicated by white boxes in (c)). First-derivative zero crossings show the time of maximal photoacoustic contrast inflow and outflow points as indicated by solid and hollow arrows, respectively. e) Rate of contractile motion within the indicated ROI. f) Representative maximum intensity projection PET images of [64]Cu Pheo ss-InFroMs at different time points. g) Fecal clearance of Pheo ss-InFroMs based on Pheo itself or chelated ^{64}Cu, in mice 24 h after gavage of 100 O.D. of ss-InFroMs. h) Biodistribution of [^{64}Cu] chelated in Pheo ss-InFroMs 24 h after gavage of 100 O.D. Pheo ss-InFroMs. Error bars show mean +/− std. dev. for n=3.

COMMUNICATION

100% from feces after 24 h whereas only 70% of Chl was recovered (Figure 2b). The improved stability of Pheo ss-InFroMs probably arises from the higher hydrophobicity of Pheo, leading to more stable ss-InFroMs, driven by hydrophobic interactions.

The preliminary safety of Pheo ss-InFroMs for the use as an oral contrast agent was examined in vitro and in vivo. As shown in Figure S4 (Supporting Information), no toxicity to human epithelial colorectal adenocarcinoma (Caco-2) cell lines was observed up to calculated absorption of 100 (highest level tested) whereas the methylene blue dye induced toxicity when incubated in cell media with an absorbance of 1. Biodistribution for mice orally administered Pheo ss-InFroMs after 24 h showed no detectable Pheo in main organs including liver, spleen, kidney, heart, lung, brain, and also serum. This was not surprising since almost all the nanoparticles were recoverable from feces (Figure 2c). Encouraged by these results, we administered 100 O.D. orally to each mouse. After 24 h, GI tract and organs were extracted and histology analysis was carried out. No significant acute inflammatory response was induced by Pheo ss-InFroMs as the intestinal villi and crypts seemed intact and healthy, shown in Figure 2d. Similarly, no noticeable toxicity was observed in main organs, which appeared similar to those of control mice given phosphate buffered saline (PBS) (Figure 2e).

We used Pheo ss-InFroMs for bioimaging. As shown in **Figure 3**a, feces that were collected around 3–4 h after gavage of 100 O.D. of Pheo ss-InFroMs were highly fluorescent, whereas feces from the control group without gavage of any contrast agent exhibited no fluorescence. Fluorescence distribution in intestine could be clearly observed after gavage of Pheo ss-InFroMs whereas no signal was detected before gavage of the contrast agent or after gavage of Chl ss-InFroMs (Figure 3b). The utility of Pheo ss-InFroMs for PA imaging was then assessed. As shown in Figure 3c, contrast agent distribution in the gut was clearly observed. For functional intestinal imaging, a region of interest (ROI) was selected as indicated in Figure 3c. The PA signal within the ROI fluctuated due to peristaltic intestine movement, representing the inflow (indicated by hollow arrows) or outflow (indicated by solid arrows) of the Pheo ss-InFroMs (Figure 3d). The rate of peristaltic intestinal flow was calculated to be close to 30 contractions per minute (Figure 3e).

Although PA contrast imaging has been reported beyond 10 cm in tissues, it is not yet a viable whole body imaging technique.[41] PET is a clinically established quantitative and highly sensitive imaging modality, without any limitation of tissue penetration depth. The PET isotope ^{64}Cu could be readily and efficiently (≈90% radiolabeling yield) chelated by Pheo ss-InFroMs, which are an intrinsic copper chelator. ^{64}Cu radiolabeled Pheo ss-InFroMs showed excellent chelation stability in simulated gastric fluid and simulated intestinal fluid, as determined by the retained radioactivity in those conditions (Figure S5, Supporting Information). 100 O.D. of ^{64}Cu radiolabeled Pheo ss-InFroMs (≈10.2 MBq) was orally administered per mouse. As shown in Figure 3f, at 30 min, radioactivity was seen in the stomach and upper intestine until 4 h post gavage. As [^{64}Cu] Pheo ss-InFroMs moved down to the large intestine, the signal became attenuated, with very little remaining in the body by 24 h. Gamma counting demonstrated that close to 93% [^{64}Cu] of the administered Pheo ss-InFroMs

were recovered in feces, as shown in Figure 3g. The slight difference in biodistribution of ^{64}Cu within the Pheo informs and Pheo itself in unlabeled Pheo ss-InFroMs was likely due to a low level of dechelation of ^{64}Cu from Pheo. Minimal amount of radioactivity retained in all organs with less than 2.5% injected dose per gram tissue as shown in Figure 3h.

The fluorescence and absorption of radiolabeled [^{64}Cu] Pheo ss-InFroMs were examined. After ^{64}Cu labeling, ss-InFroMs still remained highly fluorescent (Figure S6, Supporting Information) and no changes were induced in absorption properties (Figure S7, Supporting Information). Although copper chelation results in quenching of porphyrin fluorescence,[42–44] only a small amount of ^{64}Cu is required for radiolabeling (0.4 nmol was used in these experiments). In addition, based on visible light emitted by radionuclides, [^{64}Cu] Pheo ss-InFroM displayed potential for Cerenkov imaging as yet another imaging modality for the intestine, as shown in Figure S8 (Supporting Information).

In summary, Pheo was generated following simple acidification of Chl to remove the central magnesium and was then were well-suited for surfactant-stripped micelle formation. Owing to the increase of hydrophobicity, Pheo ss-InFroMs were more stable in the GI tract compared to Chl ss-InFroMs. Pheo ss-InFroMs safely passed through the GI tract and were excreted in feces without inducing any acute toxicity to intestine and main organs. By removing the central metal, fluorescence of Pheo ss-InFroMs was unexpectedly restored, enabling fluorescence imaging of intestine. These studies show proof of principle for multimodal FL, PA, and PET gut imaging using surfactant-stripped micelles of Pheo, which is a pigment naturally consumed in human diets already.

Experimental Section

Materials: Materials were obtained from Sigma unless noted otherwise.

Dechelation of Chl: 50 mg Chl (Juntec, Japan) was dissolved in 100 mL diethyl ether (Fisher, #153099), then 1 mL 1 M hydrochloride acid (Fisher, #135078) was added dropwise with stirring for 3 h. 40 mL distilled water was then added to the diethyl ether solution to extract salts. Extraction was repeated another two times. Subsequently, Pheo containing diethyl ether was subjected to rotary evaporation and the dried materials were dissolved in a small amount of DCM. Pheo was recovered after adding methanol with the DCM solution. The precipitate was recovered and put in vacuum overnight to remove residual solvent. Approximately 75% conversion yield was achieved.

Preparation of Pheo ss-InFroMs: 10 mg Pheo was dissolved in 50 mL DCM, and then added to a 250 mL 10% (w/v) aqueous solution of Pluronic F127 (Sigma, P2443-1KG) with stirring overnight in the dark. The solution was centrifuged at 4500 ×g for 10 min and no pellet was observed. For small-scale F127 removal process (Figure 1d), 5 mL of the solution was subject to centrifugal filtration (Fisher #UFC9-100-24) at 4 °C until ≈200 μL solution was retained. Water was added back to the concentrate and the washing procedure was repeated three times. For large-scale washing, filtration (Sartorius vivaflow, 1501008VS) assembled with peristalsis pump (Masterflex L/S) and tubing (masterflex 6434-16) was used to remove excess Pluronic F127. To reach lower temperature and maximize F127 removal, membranes modules, tubing, and solutions to be washed were immersed in ice. The solution was finally concentrated with centrifugal filtration (Fisher #UCF9-100-24) to required concentration.

Characterization of ss-InFroMs: Absorbance was measured with a Lambda 35 UV–Vis or a Lambda XLS spectrophotometer (PerkinElmer)

using cuvettes with 1 cm path length for regular absorbance measurement or 10 µm path-length cuvette for high concentration spectral shifting analysis. XRD was measured on a Rigaku Ultima IV, with a scanning speed of $0.5°$ min^{-1} at a 0.03 interval. Calculated absorbance was the calculated actual optical absorbance of concentrated Pheo ss-InFroMs for a 1 cm path length cuvette. For 1 cm path length measurements, calculated absorbance equaled the absorbance of the diluted solution times the dilution factor; for 10 µm path length measurements, calculated absorbance was absorbance as measured times 1000 (converted to 1 cm path length). For fluorescence spectra, ≈10 µL Chl or Pheo ss-InFroMs were diluted in 2 mL distilled water or ethanol, absorbance at 420 nm was adjusted to be the same then fluorescence was measured on a fluorometer (Photon Technology International). 420 nm was used as the excitation wavelength. For relative quantum yield calculation, the integrated area between 650 and 800 nm emission was used. Fluorescence images were taken on IVIS Lumina II system. Transmission electron microscopy was performed using a JEM-2010 electron microscope with 1% uranyl acetate staining. Mass spectra were obtained using a ThermoFinnigan MAT95XL instrument. Dynamic light scattering measurement was conducted on a Nano ZS 90 Zetasizer (Malvern Instruments). For molar ratio calculations, Pheo ss-InFroMs were freeze dried after absorbance measurement. Then acetone was added to the powder for the determination of the mass of dye by measuring the absorbance. F127 concentrations were determined by the cobalt thiocyanate assay. Briefly, cobalt thiocyanate was prepared by dissolving 0.3 g cobalt nitrate hexahydrate and 1.2 g ammonium thiocyanate in 3 mL water. Then 100 µL of cobalt thiocyanate, 40 µL F127 solution in the concentration range of 0–7.5 wt% (more concentrated F127 solutions were diluted to fit that range), 200 µL ethyl acetate, and 80 µL ethanol were combined. The mixture was vortexed and centrifuged at $14\,000 \times g$ for 1 min. The supernatant was removed and the blue pellet was washed using ethyl acetate several (approximately five) times until the supernatant became colorless. The pellet was then dissolved in 1 mL acetone to measure the absorbance at 623 nm. For the washing curve in Figure 1d, F127 concentration was quantified as above and dye retentions were calculated by measuring the absorbance of filtrates. To assess the stability of Chl or Pheo ss-InFroMs or ^{64}Cu radiolabeled Pheo ss-InFroMs in simulated intestinal fluid (SIF), ss-InFroMs was dialyzed against 200 mL pancreatin-containing SIF (Ricca, #7109-32). Concentrated ss-InFroMs were diluted with SIF so that the absorbance was close to 1, then dialyzed at 37 °C. Absorbance (for nonradiolabeled nanoparticles) or radioactivity (for radiolabeled nanoparticles) was measured at different time points as shown in figures.

Cell Viability: Caco-2 cells were maintained in Dulbecco's Modified Eagle Medium containing 20% fetal bovine serum and 1% penicillin/streptomycin at 37 °C under 5% CO_2. Cells were seeded at a concentration of 1×10^4 cells per well. Cells were allowed to attach in media containing serum for 24 h. Samples were added to the wells and incubated for 24 h. Media was removed and washed twice with PBS gently. Immediately, PBS containing 2,3-bis(2-methoxy-4-nitro-5-sulfophenyl)-2H-tetrazolium-5-carboxanilide (XTT) (50 µg mL^{-1}) and *N*-methyl dibenzopyrazine methyl sulfate at 50 and 60 µg mL^{-1}, respectively, were added to each well. Plate absorbance was read 2 h later at 450 and 630 nm. Cell viability was calculated for the treated cells with respect to untreated control cells. XTT assays were performed in triplicates.

Animal Studies: Animal experiments were performed in accordance with the University at Buffalo or the University of Wisconsin–Madison Institutional Animal Care and Use committees. Six to eight weeks female ICR mice (Envigo) were used for all experiments. 100 O.D. of Pheo or Chl ss-InFroMs were gavaged in mice that had been fasted overnight. For fecal imaging, feces were collected ≈4 h after gavage for fluorescence or photoacoustic imaging. Mice in control groups were given no contrast agent. To determine recovery percentage of Pheo in feces, feces were dissolved in 2 mL chloroform followed by homogenization and centrifugation at $3000 \times g$ for 3 min and absorbance at 660 nm of supernatants was measured. Biodistribution of nonradiolabeled Pheo ss-InFroMs was quantified using the same protocol. For histological studies, organs or intestines were immersed in 10% neutral buffered formalin (VWR #16004-114) and fixed over 24 h. The fixed organs were processed through increasing grades of alcohol, cleared in xylene, and infiltrated with paraffin (TBS), they were subsequently embedded, cut, and stained with haematoxylin and eosin. Finally, the slides were scanned with single slide scanner (Aperio).

Intestinal Imaging: For all three imaging methods (FL, PACT, PET), 100 O.D. of Pheo or Chl ss-InFroM was gavaged in mice that had been fasted overnight. For fluorescence imaging of intestine, images were acquired in an IVIS Lumina II system 3 h post gavage with the mice anesthetized. Control groups were gavaged Chl ss-InFroMs or nothing. For photoacoustic imaging of the intestine, a 672 nm excitation light was provided by an Nd:YAG laser with a 10 ns pulse duration and 10 Hz pulse repetition rate. The output of the laser was routed to the imaging region through a 1.2 cm diameter fiber bundle. The maximum light intensity at the skin surface was around 12 mJ cm^{-2}, which is below the American National Standards Institute (ANSI) safety limitation of 20 mJ cm^{-2}. The photoacoustic signal was detected by a 128-element linear transducer array (5 MHz central frequency ATL/Philips L7-4). The received signals were first amplified by 54 dB and then digitized by a 128-channel ultrasound data acquisition system (Vantage, Verasonics) with 20 MHz sampling rate. The raw channel data were reconstructed using the universal back-projection algorithm[45] and the reconstructed image could be displayed in real-time during the experiment. For PET imaging, ^{64}Cu was produced via a $^{64}Ni(p,n)^{64}Cu$ reaction using an onsite cyclotron (GE PETrace) at the University of Wisconsin–Madison. For radiolabeling, 37 MBq of $^{64}CuCl_2$ was diluted in 300 µL of 0.1 M sodium acetate buffer, (pH 5.5) and added to 400 O.D. nanonaps. The mixture was incubated at 37 °C for 60 min with constant shaking, followed by the purification by Amicon Ultra-4 centrifugal filter unit (Millipore) using PBS. PET scanning was conducted using an Inveon microPET/microCT rodent model scanner (Siemens Medical Solutions USA, Inc.). ICR mice were fasted overnight and gavaged with 100 O.D. pheophytin ss-InFroMs. Static PET scans were performed at indicated time-points postinjection. All PET images were reconstructed using a maximum a posteriori algorithm, without attenuation or scatter correction, and analyzed with Inveon Research Workplace software. 24 h post gavage, all mice were sacrificed and organs and intestines were harvested and wet-weighted. The radioactivity in the tissue was measured by WIZARD^2 gamma counter (PerkinElmer) for radiolabel biodistribution.

Supporting Information

Supporting Information is available from the Wiley Online Library or from the author.

Acknowledgements

[1] J. Kim, Y. Piao, T. Hyeon, *Chem. Soc. Rev.* **2009**, *38*, 372.
[2] J. Rieffel, U. Chitgupi, J. F. Lovell, *Small* **2015**, *11*, 4445.
[3] H.-Y. Lee, Z. Li, K. Chen, A. R. Hsu, C. Xu, J. Xie, S. Sun, X. Chen, *J. Nucl. Med.* **2008**, *49*, 1371.
[4] W. Cai, K. Chen, Z.-B. Li, S. S. Gambhir, X. Chen, *J. Nucl. Med.* **2007**, *48*, 1862.
[5] J. Lin, M. Wang, H. Hu, X. Yang, B. Wen, Z. Wang, O. Jacobson, J. Song, G. Zhang, G. Niu, P. Huang, X. Chen, *Adv. Mater.* **2016**, *28*, 3273.

[6] Q. Fan, K. Cheng, X. Hu, X. Ma, R. Zhang, M. Yang, X. Lu, L. Xing, W. Huang, S. S. Gambhir, Z. Cheng, *J. Am. Chem. Soc.* **2014**, *136*, 15185.

[7] X. Zhu, J. Zhou, M. Chen, M. Shi, W. Feng, F. Li, *Biomaterials* **2012**, *33*, 4618.

[8] J. Kim, H. S. Kim, N. Lee, T. Kim, H. Kim, T. Yu, I. C. Song, W. K. Moon, T. Hyeon, *Angew. Chem. Int. Ed.* **2008**, *47*, 8438.

[9] S. Xue, Y. Wang, M. Wang, L. Zhang, X. Du, H. Gu, C. Zhang, *Int. J. Nanomed.* **2014**, *9*, 2527.

[10] W. Koba, L. A. Jelicks, E. J. Fine, *Am. J. Pathol.* **2013**, *182*, 319.

[11] A. H. Iagaru, E. S. Mittra, I. R. McDougall, A. Quon, S. S. Gambhir, *Nucl. Med. Commun.* **2008**, *29*, 1046.

[12] A. Iagaru, E. Mittra, D. W. Dick, S. S. Gambhir, *Mol. Imaging Biol.* **2011**, *14*, 252.

[13] L. Cheng, J. Liu, X. Gu, H. Gong, X. Shi, T. Liu, C. Wang, X. Wang, G. Liu, H. Xing, W. Bu, B. Sun, Z. Liu, *Adv. Mater.* **2014**, *26*, 1886.

[14] J. Qiu, Q. Xiao, X. Zheng, L. Zhang, H. Xing, D. Ni, Y. Liu, S. Zhang, Q. Ren, Y. Hua, K. Zhao, W. Bu, *Nano Res.* **2015**, *8*, 3580.

[15] K. Cheng, S.-R. Kothapalli, H. Liu, A. L. Koh, J. V. Jokerst, H. Jiang, M. Yang, J. Li, J. Levi, J. C. Wu, S. S. Gambhir, Z. Cheng, *J. Am. Chem. Soc.* **2014**, *136*, 3560.

[16] D. R. Arifin, C. M. Long, A. A. Gilad, C. Alric, S. Roux, O. Tillement, T. W. Link, A. Arepally, J. W. M. Bulte, *Radiology* **2011**, *260*, 790.

[17] I.-C. Sun, D.-K. Eun, H. Koo, C.-Y. Ko, H.-S. Kim, D. K. Yi, K. Choi, I. C. Kwon, K. Kim, C.-H. Ahn, *Angew. Chem. Int. Ed.* **2011**, *50*, 9348.

[18] Y. Li, T. Lin, Y. Luo, Q. Liu, W. Xiao, W. Guo, D. Lac, H. Zhang, C. Feng, S. Wachsmann-Hogiu, J. H. Walton, S. R. Cherry, D. J. Rowland, D. Kukis, C. Pan, K. S. Lam, *Nat. Commun.* **2014**, *5*, 4712.

[19] K. Pu, A. J. Shuhendler, J. V. Jokerst, J. Mei, S. S. Gambhir, Z. Bao, J. Rao, *Nat. Nanotechnol.* **2014**, *9*, 233.

[20] K. Pu, J. Mei, J. V. Jokerst, G. Hong, A. L. Antaris, N. Chattopadhyay, A. J. Shuhendler, T. Kurosawa, Y. Zhou, S. S. Gambhir, Z. Bao, J. Rao, *Adv. Mater.* **2015**, *27*, 5184.

[21] Q. Miao, Y. Lyu, D. Ding, K. Pu, *Adv. Mater.* **2016**, *28*, 3662.

[22] Y. Lyu, Y. Fang, Q. Miao, X. Zhen, D. Ding, K. Pu, *ACS Nano* **2016**, *10*, 4472.

[23] N. Mitchell, T. L. Kalber, M. S. Cooper, K. Sunassee, S. L. Chalker, K. P. Shaw, K. L. Ordidge, A. Badar, S. M. Janes, P. J. Blower, M. F. Lythgoe, H. C. Hailes, A. B. Tabor, *Biomaterials* **2013**, *34*, 1179.

[24] G. J. Strijkers, E. Kluza, G. A. F. V. Tilborg, D. W. J. van der Schaft, A. W. Griffioen, W. J. M. Mulder, K. Nicolay, *Angiogenesis* **2010**, *13*, 161.

[25] J. Rieffel, F. Chen, J. Kim, G. Chen, W. Shao, S. Shao, U. Chitgupi, R. Hernandez, S. A. Graves, R. J. Nickles, P. N. Prasad, W. Cai, J. F. Lovell, *Adv. Mater.* **2015**, *27*, 1785.

[26] Y. Sun, X. Zhu, J. Peng, F. Li, *ACS Nano* **2013**, *7*, 11290.

[27] J.-W. Shen, C.-X. Yang, L.-X. Dong, H.-R. Sun, K. Gao, X.-P. Yan, *Anal. Chem.* **2013**, *85*, 12166.

[28] X. Wu, G. Chen, J. Shen, Z. Li, Y. Zhang, G. Han, *Bioconjugate Chem.* **2015**, *26*, 166.

[29] G. Chen, H. Qiu, R. Fan, S. Hao, S. Tan, C. Yang, G. Han, *J. Mater. Chem.* **2012**, *22*, 20190.

[30] Y. Zhang, M. Jeon, L. J. Rich, H. Hong, J. Geng, Y. Zhang, S. Shi, T. E. Barnhart, P. Alexandridis, J. D. Huizinga, M. Seshadri, W. Cai, C. Kim, J. F. Lovell, *Nat. Nanotechnol.* **2014**, *9*, 631.

[31] C. Lee, J. Kim, Y. Zhang, M. Jeon, C. Liu, L. Song, J. F. Lovell, C. Kim, *Biomaterials* **2015**, *73*, 142.

[32] Y. Zhang, W. Song, J. Geng, U. Chitgupi, H. Unsal, J. Federizon, J. Rzayev, D. K. Sukumaran, P. Alexandridis, J. F. Lovell, *Nat. Commun.* **2016**, *7*, 11649.

[33] S. Kwon, E. M. Sevick-Muraca, *Neurogastroenterol. Motil.* **2011**, *23*, 881.

[34] Y. Zhang, J. F. Lovell, *Theranostics* **2012**, *2*, 905.

[35] H. Huang, W. Song, J. Rieffel, J. F. Lovell, *Front. Phys.* **2015**, *3*, 23.

[36] M. G. Ferruzzi, J. Blakeslee, *Nutr. Res.* **2007**, *27*, 1.

[37] R. C. Martins, M. G. Almeida, C. L. M. Silva, *Int. J. Refrig.* **2004**, *27*, 850.

[38] X. Huang, K. Nakanishi, N. Berova, *Chirality* **2000**, *12*, 237.

[39] I. V. Tetko, V. Y. Tanchuk, *J. Chem. Inf. Comput. Sci.* **2002**, *42*, 1136.

[40] H. Huang, X. Liu, T. Hu, P. K. Chu, *Biosens. Bioelectron.* **2010**, *25*, 2078.

[41] Y. Zhou, D. Wang, Y. Zhang, U. Chitgupi, J. Geng, Y. Wang, Y. Zhang, T. R. Cook, J. Xia, J. F. Lovell, *Theranostics* **2016**, *6*, 688.

[42] H. Huang, W. Song, G. Chen, J. M. Reynard, T. Y. Ohulchanskyy, P. N. Prasad, F. V. Bright, J. F. Lovell, *Adv. Healthcare Mater.* **2014**, *3*, 891.

[43] S. Shao, J. Geng, H. Ah Yi, S. Gogia, S. Neelamegham, A. Jacobs, J. F. Lovell, *Nat. Chem.* **2015**, *7*, 438.

[44] K. A. Carter, S. Wang, J. Geng, D. Luo, S. Shao, J. F. Lovell, *Mol. Pharm.* **2016**, *13*, 420.

[45] M. Xu, L. V. Wang, *Phys. Rev. E: Stat., Nonlinear, Soft Matter Phys.* **2005**, *71*, 16706.